

RoMe: Towards Large Scale Road Surface Reconstruction via Mesh Representation

Ruohong Mei^{1*}, Wei Sui¹, Jiaxin Zhang^{1*}, Qian Zhang¹, Tao Peng² and Cong Yang^{2†}

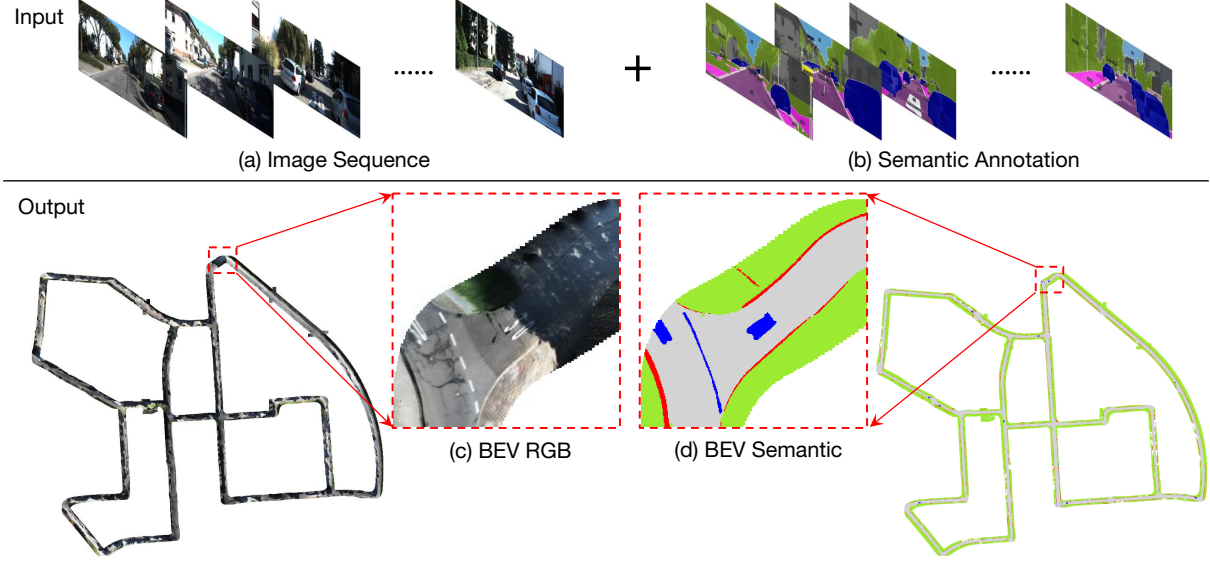


Fig. 1: Road surface reconstruction results (KITTI odometry sequence-00, area of approximately 600×600 square meters) with our proposed RoMe. The first row presents the input image sequence with semantic annotations. The second row illustrates the final results with close-up details (red rectangles): the reconstructed surface (BEV RGB) and its correlated semantics (BEV Semantic).

Abstract—Large-scale road surface reconstruction is becoming important to autonomous driving systems, as it provides valuable training and testing data effectively. In this paper, we introduce a simple yet efficient method, RoMe, for large-scale Road surface reconstruction via Mesh representations. To simplify the problem, RoMe decomposes a 3D road surface into a triangle-mesh and a multilayer perception network to model the road elevation implicitly. To retain fine surface details, each mesh vertex has two extra attributes, namely color and semantics. To improve the efficiency of RoMe in large-scale environments, a novel waypoint sampling method is introduced. As such, RoMe can properly preserve road surface details, with only linear computational complexity to road areas. In addition, to improve the accuracy of RoMe, extrinsics optimization is proposed to mitigate inaccurate extrinsic calibrations. Experimental results on popular public datasets also demonstrate the high efficiency and accuracy of RoMe.

I. INTRODUCTION

Recently, bird-eye-view (BEV) perception has become popular in autonomous driving, as its output space is naturally consistent with downstream tasks such as planning and control. Accordingly, large-scale road surface reconstruction

becomes more important for its potential applications in providing training and validating data for BEV perception tasks. Commonly used road surface reconstruction methods can be roughly categorized into two clusters: traditional methods [1], [2] and neural radiance field (NeRF)-based methods [3]–[6].

Traditional MVS (multi-view stereo) methods usually reconstruct dense (or semi-dense) points. The reconstruction results are normally promising for the Lambert surface. However, for textureless road surface, their results are usually noisy and incomplete. Besides, these methods require huge computing resources for large-scale reconstruction (e.g. 600×600 square meters). Recently, implicit representation-based methods have been actively used in photorealistic reconstruction on road surface reconstruction with only a series of posed images (images with camera poses) [4]–[6]. These methods adopt one or more implicit representations such as MLP (Multi-Layer Perceptions) to reconstruct the whole city scene. To do so, most of them are supervised by depth information from Lidar and pure-vision. However, due to the high resource consumption of whole 3D space sampling and accumulated rendering, their usage is limited in large-scale scenarios.

In practice, a 3D road surface is usually not watertight, which means it can be separately represented in the form of a smooth mesh with pixel-level elevation. Motivated by

¹ Ruohong Mei, Jiaxin Zhang, Wei Sui and Qian Zhang are with Horizon Robotics, Haidian District, Beijing, China. {ruohong.mei, jiaxin02.zhang, wei.sui, qian01.zhang}@horizon.ai. * Equal contribution.

² Tao Peng and Cong Yang are with School of Future Science and Engineering, Soochow University, Suzhou, China. {tpeng@suda.edu.cn, yangcong955@126.com}. † Corresponding author.

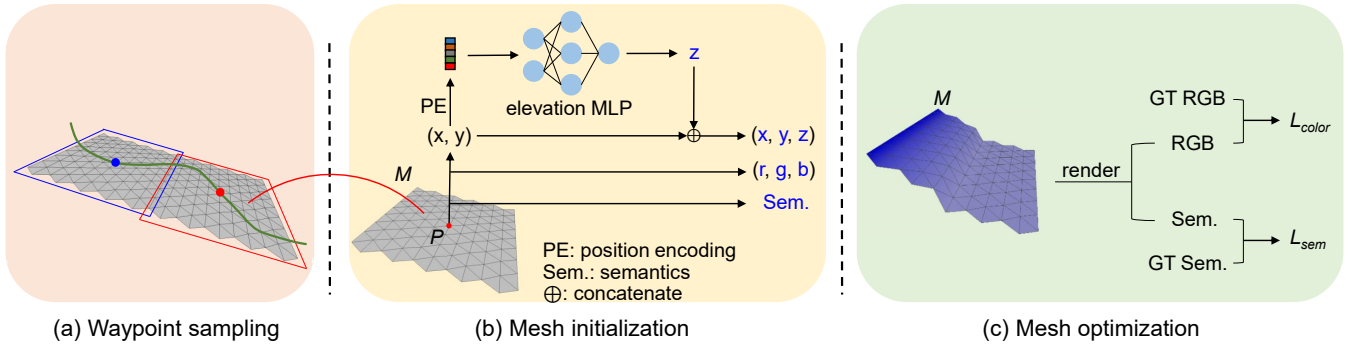


Fig. 2: RoMe overview. (a) Waypoint sampling for training acceleration. The green line presents the camera trajectory, while red and blue boxes are adjacent subareas. The red and blue dots are waypoint samples. (b) Mesh initialization. With initialization of mesh M , each vertex is assigned with position (x, y, z) , color (r, g, b) , and semantics. Vertex elevation z is optimized via an elevation MLP network. (c) Mesh optimization. L_{color} and L_{sem} are the targets to optimize, therefore M can be rendered to RGB images and correlated semantics. Thus, parameters $(z, (r, g, b) \text{ and } Sem.)$, marked blue in (b)) are jointly optimized to get the final reconstructed road mesh M .

this, we design a simple yet efficient pure-vision method, RoMe, for large-scale road surface reconstruction. Fig. 1 shows a concise pipeline of our method: given a sequence of posed images and corresponding semantic annotations as input, RoMe builds the whole large-scale 3D textured road mesh, namely BEV RGB and BEV semantics. In particular, each mesh vertex has primitives of elevation, colors, and semantics. Colors and semantics are the parameters to be optimized directly. The elevation of each vertex is a function of its location (x, y) expressed by the MLP network. The rationale behind such representation is that by tuning the frequency of position encoding, we can easily control the smoothness of the elevation, in case fierce elevation changes occur. To further improve training efficiency and save resources, we also introduce a waypoint sampling method to speed up the optimizing process (see Fig. 2 (a) and (b)). In addition, camera extrinsics will not be always unchanged which are susceptible to weather conditions, collisions and so on. Therefore, it is necessary to optimize camera extrinsics when reconstructing the road surface.

The main contributions of this work are as follows: (1) We propose a simple yet efficient framework, RoMe, to reconstruct large-scale three-dimensional road surfaces with textures and semantics. (2) Benefiting from the proposed road surface mesh representations and waypoint sampling strategies, the computational efficiency of reconstruction is dramatically improved. (3) Extrinsics optimization is proposed to rectify incorrect camera rigs, resulting in better reconstruction. Both qualitative and quantitative experiments on public datasets demonstrate the accuracy and robustness of our proposed methods.

II. RELATED WORKS

A. Multi-View Stereo

3D reconstruction has been extensively studied in recent decades [7]. However, the results of traditional MVS methods severely depend on feature points extraction and matching, which limits their performance in texture-less scenes [1], [2]. This is critical for driving-road reconstruction, while

feature points from road areas are normally sparse and unbalanced. Although [8]–[10] were specifically designed for road surface reconstruction, they only focus on a fine-grained surface within certain small areas. As a result, it is difficult to apply them in large-scale scenarios.

There are also some traditional MVS methods that can be applied to large-scale (even city-level) scenes [11]. Most of them follow a certain paradigm: extract correspondent points from images, reconstruct sparse 3D points through point matching and bundle adjustments, and finally create mesh based on points. These methods usually focus on reconstructing whole building details and often fail to create the mesh of textureless surfaces such as roads.

Different from existing approaches, our proposed RoMe can reconstruct the whole road surface regardless of the richness of textures. Moreover, our method can effectively reconstruct large-scale road surface and properly preserve features including textures, semantics, and elevation.

B. Surface Reconstruction

For specific applications such as road surface reconstruction, general MVS methods are not computation efficient as they model whole scenes through dense pointclouds. The textured-surface is obviously a better choice for this specific task. Previous road surface reconstruction works can be roughly divided into explicit and implicit ways. For explicit surface reconstruction: Tong *et al.* proposed a cloud-sourcing system that can build large-scale semantic maps with low-cost production cars using cameras [12]. However, such methods highly rely on inverse perspective mapping (IPM) and are insensitive to elevation changes on the road surface. Besides, they only recover structureless semantic point clouds. Focusing on surface reconstruction, rendering-based methods [13], [14] adopt mesh representation with view-dependent appearances. For implicit surface reconstruction, the recently proposed NeRF [3] adopts implicit representation and voxel rendering, achieving high-fidelity rendering results. Here, we briefly glance through neural implicit representations on large street view. Large-scale NeRF aims to recover the whole city block (or driving scene) while

maintaining details such as buildings and vegetation along the street. To do so, these methods [4]–[6] usually have extra requirements during data acquisition: either requiring LiDAR, or extremely large amounts of images with different viewing angles. In contrast, our proposed method only requires several surrounding vehicle cameras (or even single front-facing camera). As a result, our method can be easily applied to any common autonomous-driving platforms such as nuScenes [15] and KITTI [16]. Furthermore, waypoint sampling can effectively speed up training and reduce resource consumption (positively verified in Section IV).

III. APPROACHES

Given a sequence of posed images, RoMe reconstructs both road surface textures and semantics. As shown in Fig. 2, RoMe is composed of three parts: Waypoint Sampling, Mesh Initialization, and Mesh Optimization. For brief presentation, extrinsics optimization is not shown in Fig. 2 and we will demonstrate it together with waypoint sampling in III-B

A. Mesh Initialization

In RoMe, the meshes are initialized based on the estimated camera poses from ORB-SLAM2 [17] (or COLMAP [1]). Built on that, the semantic segmentation method [18] is employed to generate semantics including roads, curbs, sign lanes, vehicles, etc. As a by-product, these semantics are also used to mask out all movable objects such as vehicles and pedestrians. This is because such dynamic objects could badly break the consistency of the whole road structure.

In Fig. 2, the initialized flat mesh consists of equilateral triangles and faces, denoted by M . Each face has three vertices. Each vertex P has three attributes: location (x, y, z) , color (r, g, b) and semantics. The position encoding is applied on (x, y) , thereby feeding them into the elevation MLP to obtain predictions of elevation z :

$$z = \text{MLP}(\text{PE}(x, y)) \quad . \quad (1)$$

where PE denotes position encoding. The rationale behind $\text{MLP}(\cdot)$ is that, compared with textures and semantics, the elevation of road surface has a relatively low spatial frequency. Thus, MLP instead of learnable parameters, is used for elevation estimation to limit drastic elevation changes. Besides, we can easily control the smoothness of road surface by simply changing the frequency of PE.

B. Optimizing Strategies

Waypoint Sampling. To accelerate the reconstruction of large areas with multiple blocks (e.g. 600 * 600 square meters), we propose a novel sampling method, namely waypoint sampling (detailed in Algorithm 1). It can dramatically reduce the computational resources. The core idea is: *Divide and Conquer*. Specifically, camera pose positions are regarded as a set of point clouds P . The first waypoint is randomly selected from P . Given the desired sampling radius R , the farthest point sampling algorithm is applied to P and selects waypoints (p_1, p_2, \dots, p_N) . After that, two steps are followed: (1) gathering all camera poses P_{sub_j} and

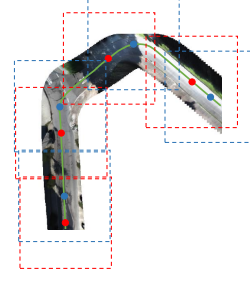


Fig. 3: Waypoint sampling. The green line denotes the camera trajectory. Dots and correlated boxes represent different sampled waypoints and subareas in different epochs (in different colors).

Algorithm 1 Waypoint Sampling

Input:

All camera poses, P ;
All camera images, I ;
Waypoint radius, R ;

Output:

N waypoints, p_1, p_2, \dots, p_N ;
 N corresponding: subsets of areas $(A_{sub_1}, A_{sub_2}, \dots, A_{sub_N})$;
subsets of camera poses $(P_{sub_1}, P_{sub_2}, \dots, P_{sub_N})$;
subsets of images $(I_{sub_1}, I_{sub_2}, \dots, I_{sub_N})$;

for loop i in range(loops) **do**

$p_1 \leftarrow \text{random select}(P)$;

$p_2, p_3, \dots, p_N \leftarrow \text{farthest point sampling}(p_1, R)$;

for waypoint j in waypoints **do**

$A_{sub_j} \leftarrow \text{square}(p_j, R)$;

$P_{sub_j} \leftarrow P \text{ inside } A_{sub_j}$;

$I_{sub_j} \leftarrow I \text{ inside } A_{sub_j}$;

Cut off gradient backward outside A_{sub_j} ;

Train and optimize;

end for

end for

images I_{sub_j} within the radius for each waypoint p_j . (2) Traverse each subarea A_{sub_j} for optimization (forwards and backwards process), while the remaining subareas are frozen. The second step is iteratively applied until all subareas are properly covered. As a result, the whole road surface is updated accordingly.

In practice, to avoid inconsistency in boundaries between different sub-areas, the initial waypoint is randomly selected in each training epoch. Fig. 3 visualizes how waypoints and corresponding subareas are generated. The green line is the camera trajectory. Red and blue dots are randomly sampled waypoints in different epochs. Red and blue boxes are corresponding sub-areas.

Extrinsics Optimization: Accurate camera extrinsics are not always guaranteed, even in offline calibration systems. This is understandable since they are easily affected by multiple factors like temperature and vibrations. For instance, we observed that the extrinsics among nuScenes cameras are not always ideal in some particular scenes. For this, we decouple camera poses into vehicle ego poses and camera extrinsics w.r.t vehicle ego coordinates.

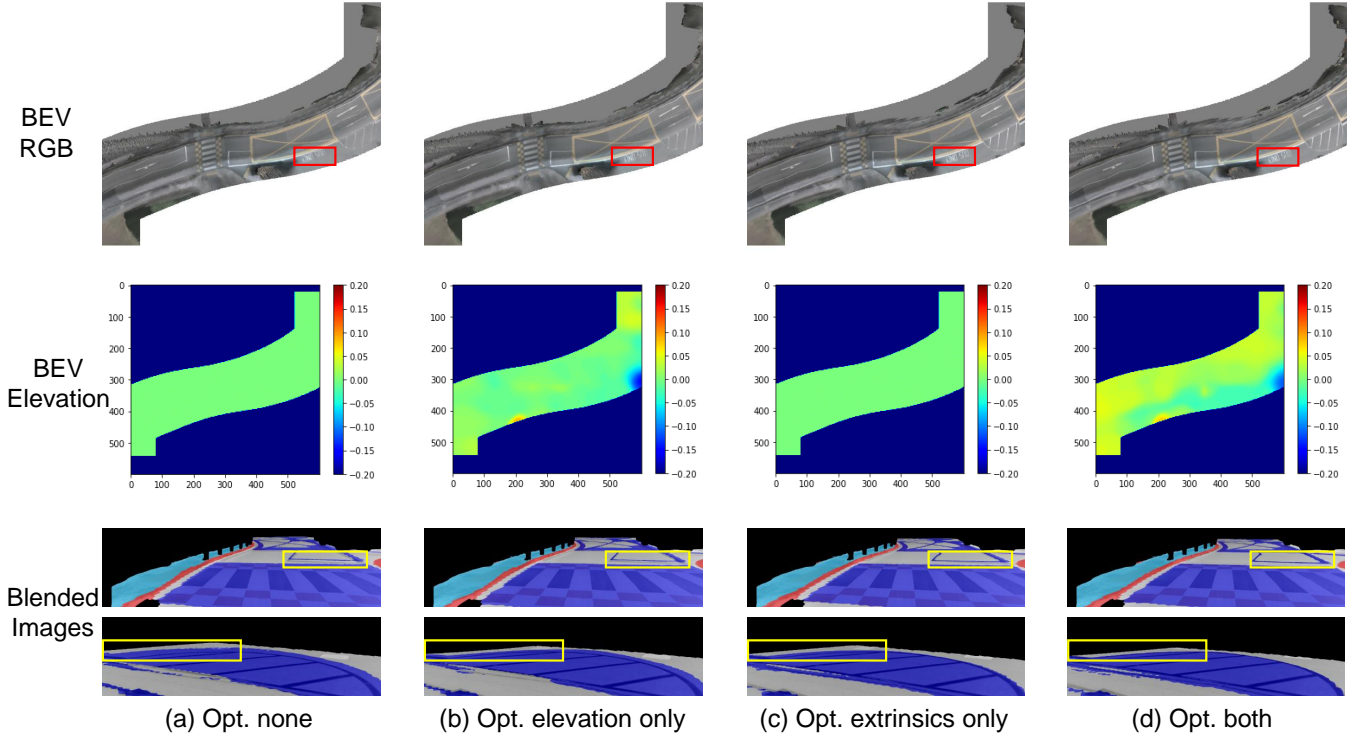


Fig. 4: Ablation studies on elevation and extrinsics. Top: BEV RGB. Middle: BEV Elevation. Bottom: Blended Images. The detailed results are in Table I. By restoring elevation and optimizing extrinsics, the results are promising and (RGB, semantics) are properly aligned.

TABLE I: Ablation study. Opt. elevation: Optimizing elevation. Opt. extrinsics: Optimizing extrinsics. With Optimizing both elevation and extrinsics, the reconstruction results are the best (marked in bold) on both textures and semantics.

Opt. elevation	Opt. extrinsics	PSNR	mIoU (%)
×	×	25.5	71.4
✓	×	25.9	73.9
×	✓	26.0	79.0
✓	✓	26.7	83.0

Camera extrinsic is expressed as a transform matrix $T = [R|t]$ in $SE[3]$, in which $R \in SO(3)$ denotes rotations and $t \in R^3$ denotes translations. Translation t can be easily optimized because it is defined in Euclidean space. Rotation R can be expressed as the axis-angle: $\phi := \alpha\omega$, $\phi \in R^3$ where α is a rotation angle and ω is a normalized rotation axis. It can be converted to R by Rodrigues' formula:

$$R = I + \frac{\sin(\alpha)}{\alpha} \phi^\wedge + \frac{1 - \cos(\alpha)}{\alpha^2} (\phi^\wedge)^2 \quad (2)$$

in which skew operator $(\bullet)^\wedge$ converts a vector ϕ to a skew matrix:

$$\phi^\wedge = \begin{pmatrix} \phi_0 \\ \phi_1 \\ \phi_2 \end{pmatrix}^\wedge = \begin{pmatrix} 0 & -\phi_2 & \phi_1 \\ \phi_2 & 0 & -\phi_0 \\ -\phi_1 & \phi_0 & 0 \end{pmatrix} \quad (3)$$

In practice, we optimize relative camera extrinsics compared with calibrated extrinsics by α , ϕ and translation t for faster and easier convergence.

C. Training Loss

To obtain training supervision, we first feed source mesh M into the differentiable renderer in [19]. Specifically, as shown in Eq. 4, we rasterize M to get rendering results of image views from the j -th camera pose π_j :

$$[C_j, S_j, D_j, Mask_j] = \text{Rasterize}(\pi_j, M) \quad (4)$$

where C_j , S_j and D_j are the j -th rendered RGB, semantic, and depth images, respectively. $Mask_j$ is the corresponding silhouette image indicating the area of supervision. $j = 1, \dots, N$. N is the maximum number of source images and corresponding poses. D_j could be supervised if sparse or dense depth is provided.

Built on Eq. 4, the color (aka. RGB) loss L_{color} and semantics loss L_{sem} are defined for training RGB images and semantics, respectively:

$$L_{color} = \frac{1}{N * \sum(Mask_j)} \sum_{j=1}^N Mask_j * |C_j - \tilde{C}_j| \quad (5)$$

$$L_{sem} = \frac{1}{N * \sum(Mask_j)} \sum_{j=1}^N Mask_j * CE(S_j, \tilde{S}_j) \quad (6)$$

where \tilde{C}_N and \tilde{S}_N denote the ground truth of RGB images and semantics, respectively. $CE(\cdot)$ refers to cross-entropy loss. During training, each vertex is optimized by multiple images from different views. Once all of them (from thousands to millions according to mesh resolution) are properly optimized, the final mesh (with elevation, colors, and semantics) is obtained to represent the whole road surface.

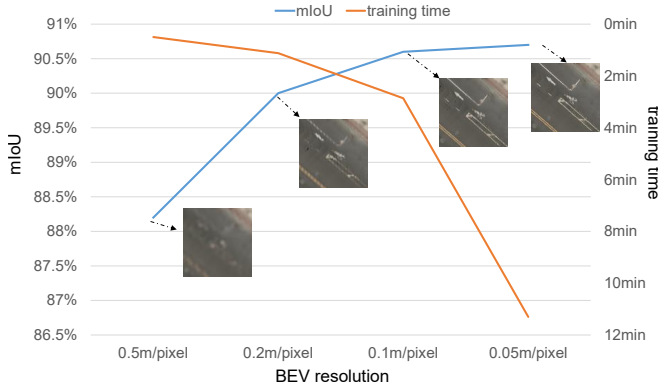


Fig. 5: Ablation study on BEV resolution. A 0.1m/pixel resolution could get realistic reconstruction and faster training speed.

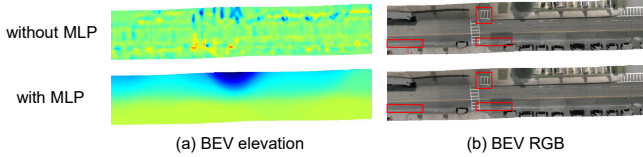


Fig. 6: Ablation study on ways of learning BEV elevation. BEV elevation is shown in colormap jet from -0.2 meters to 0.2 meters. Using MLP could get smoother elevation leading to better reconstruction as shown in red boxes.

IV. EXPERIMENTS

A. Implementation Detail

Datasets: Our proposed method was conducted on two popular driving datasets: nuScenes [15] and KITTI [16]. nuScenes is a large driving dataset that contains 1000 scenes. Each scene is a 20-second video clip annotated at 2 Hz. The camera rig comprises 6 cameras to get a full 360 degree field of view. The KITTI odometry benchmark consists of 22 sequences, with 11 training sequences (00-10) and 11 test sequences (11-21). In our work, we only use monocular images from the left RGB camera.

Metrics: The semantics were generated for all images using Mask2Former [18] (Swin-L [21] backbone, pretrained weights on the Mapillary Vistas Dataset [22]). All experiments were conducted on a Linux server with a single RTX-3090 GPU. We evaluate all approaches using the traditional image similarity metric, peak signal-to-noise ratio (PSNR) for images, and mean intersection over union (mIoU) for semantic segmentation. We use the prediction of Mask2Former as ground truth semantics, as it achieves a leading position in mainstream semantic segmentation datasets (e.g. a large-scale street-level image dataset Mapillary Vistas [22]).

Implementation: RoMe initializes a road surface mesh by [19] with RGBs, semantics and elevation. We use Adam [23] to optimize these learnable parameters and set the learning rate of RGBs and semantics to 0.1 and elevation to 0.001. Running 7 epochs in total and reducing the learning rate by half at 2nd and 4th epoch is enough for most of scenes. BEV resolution is 0.1 meter per pixel. Elevation MLP is a simple network of 8 layers with width 128 borrowed from [24].

TABLE II: Waypoint sampling. We can achieve 2x faster speed with less GPU resources after using waypoint sampling. Meanwhile, results will not be hurt.

waypoint sampling	time(min)	GPU(GB)	PSNR	mIoU(%)
×	7	15	23.4	86.7
✓	3.5	11	23.4	86.7

B. Ablation Study

Elevation and extrinsics optimization: RoMe could restore road surface elevation and optimize camera extrinsics to get more accurate reconstruction. We choose a short clip in *scene-0865* of nuScenes for ablation study. Results are detailed in Table I. Either restoring elevation or optimizing extrinsics could improve reconstruction results. Besides, segmentation results are more prone to inaccurate extrinsics. For a more intuitive understanding, some results are visualized in Fig. 4. The BEV RGB is presented in the first row. If neither elevation estimation nor extrinsics optimization is applied, the results are blurry as highlighted in red boxes. BEV elevation are visualized (with units in meters) in the second row. It can be observed that BEV elevation in Fig. 4 (d) has more jittering than others. Here, we set the position encoding frequency to 4 to make consistent elevation predictions at most areas. Last row shows blended images of rendered semantics and original images. Observing carefully the yellow boxes, without optimizing elevation and extrinsics, the rendered semantics can not be properly aligned with source images.

BEV resolution: To leverage training speed and reconstruction qualities, we conduct experiments on BEV resolution in *scene-0391* of nuScenes and results are shown in Fig. 5. Setting BEV resolution greater than or equal 0.2m/pixel results in blurry reconstructions, and less than or equal 0.05m/pixel brings unnecessary computation. Therefore, 0.1m/pixel gets best trade-off between reconstruction qualities and speed.

Waypoint sampling: To evaluate the efficiency of waypoint sampling, we construct an area of 200 * 200 square meters from KITTI odometry sequence-00. With waypoint sampling, we achieved 2x speed and less GPU memory consumption, while achieving the same reconstruction quality as shown in II. Furthermore, we reconstruct the whole area using poses parsed from ORB-SLAM2 (see Fig. 1). It only took two hours to reconstruct the whole road surface (600 * 600 square meters).

Elevation MLP network: We conduct experiments on different methods of BEV elevation representation. One is setting BEV elevation as independent optimizable parameters directly, like RGB and semantics. The other is through MLP representation. Clearly the latter one produces better results as shown in Fig. 6. We find that setting the position encoding frequency to 4 is sufficient for most scenes.

C. Evaluation on Accuracy

We compare the proposed RoMe with the vanilla NeRF [20]. To do so, a short clip in *scene-0990* of nuScenes is selected including non-key frames for higher image frame

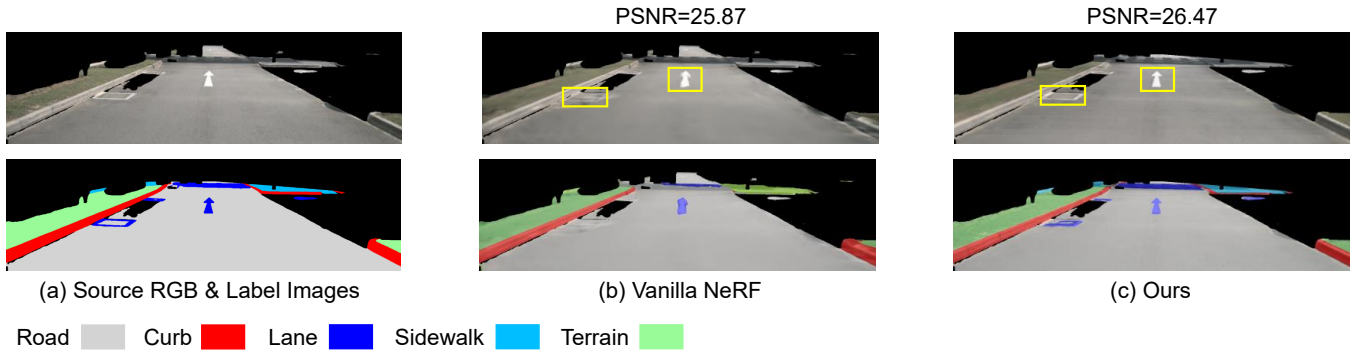


Fig. 7: RGBs and semantics reconstruction. We select a small segment from nuScenes dataset and leave out 3 frames for testing. Remaining images are used for training. As marked by the yellow boxes, our proposed RoMe preserves more details than vanilla NeRF [20].

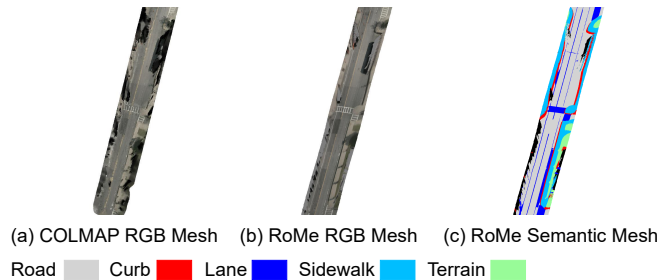


Fig. 8: Comparison with COLMAP. COLMAP will generate holes when encountering moving objects, while RoMe is robust to moving objects as it can reconstruct from other unobstructed frames. In addition, RoMe is able to reconstruct semantics at the same time.

rates. Only images from the front camera are used. Fig. 7 presents the RGB reconstruction and segmentation results. The first column contains source RGB and label image. The second column contains RGB image reconstructed by vanilla NeRF and semantics segmented by Mask2Former [18]. The third column contains RGB images and semantics reconstructed by RoMe. Our proposed method presents more realistic RGB reconstructions and precise semantics results. Road elements in yellow boxes are clearer than vanilla NeRF. In such an area of 70×70 square meters, our method only took approximately 8 minutes to converge, while the vanilla NeRF took 20 hours. The original NeRF needs to restore depth in the whole range, e.g., $0 \sim 100$ meters without depth supervision. In contrast, our method only needs to restore elevation of less than 1 meter, which is easier to optimize. Actually, mesh representation is a natural way to preserve road surface features: mostly flat and changes severely in boundaries like curbs and slope edges.

D. Evaluation on Robustness

RoMe is more robust to moving objects than COLMAP [1] as shown in Fig. 8. We choose *scene-0655* of nuScenes and mask all movable obstacles. COLMAP BEV mesh is generated by poisson mesher and is likely to generate holes when encountering moving objects. RoMe is more robust to generate complete road mesh as long as at least one frame can see road surface blocked by other frames and is able to

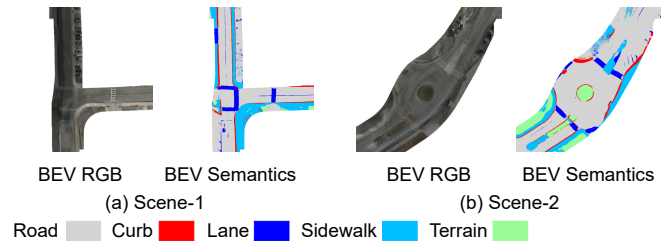


Fig. 9: Results on the nuScenes dataset. The reconstructed road surface is consistent with only immovable objects being learned.

get BEV semantics at the same time.

We can handle different scenes as long as the vehicles go through the same position. Fig. 9 shows qualitative results of multiple scenes. Both *Scene-1* and *Scene-2* consist of four individual scenes. Different scenes are combined smoothly due to precise camera poses and optimizable extrinsics. However when weather apparently differs apparently, we could only rely on semantics reconstruction as semantics are consistent under different lighting conditions in contrast to RGB images.

V. CONCLUSION

In this paper, we propose a novel framework, RoMe, for reconstructing road surfaces of large-scale environments. Its accuracy, speed, and robustness are validated via large-scale datasets (e.g. 600×600 square meters) and comparisons with the state-of-the-art methods (e.g. vanilla NeRF). In particular, based on our proposed mesh representation, road surface can be reconstructed robustly and well aligned with semantics. To accelerate training procedure and save computing resources, a waypoint sampling strategy is proposed to reconstruct road surface in subareas and smoothly join them during training. As a result, RoMe can be applied to large-scale environments. To improve the robustness of RoMe to inaccurate extrinsics calibration, an extrinsics optimization module is introduced. The data and code associated with this paper can be found at <https://to.release.after.review>.

REFERENCES

- [1] J. L. Schönberger and J.-M. Frahm, “Structure-from-motion revisited,” in *Conference on Computer Vision and Pattern Recognition (CVPR)*, 2016.

- [2] J. L. Schönberger, E. Zheng, M. Pollefeys, and J.-M. Frahm, "Pixel-wise view selection for unstructured multi-view stereo," in *European Conference on Computer Vision (ECCV)*, 2016.
- [3] B. Mildenhall, P. P. Srinivasan, M. Tancik, J. T. Barron, R. Ramamoorthi, and R. Ng, "Nerf: Representing scenes as neural radiance fields for view synthesis," in *European conference on computer vision*. Springer, 2020, pp. 405–421.
- [4] K. Rematas, A. Liu, P. P. Srinivasan, J. T. Barron, A. Tagliasacchi, T. Funkhouser, and V. Ferrari, "Urban radiance fields," in *Proceedings of the IEEE/CVF Conference on Computer Vision and Pattern Recognition (CVPR)*, June 2022, pp. 12 932–12 942.
- [5] Z. Li, L. Li, Z. Ma, P. Zhang, J. Chen, and J. Zhu, "Read: Large-scale neural scene rendering for autonomous driving," *arXiv preprint arXiv:2205.05509*, 2022.
- [6] M. Tancik, V. Casser, X. Yan, S. Pradhan, B. Mildenhall, P. P. Srinivasan, J. T. Barron, and H. Kretzschmar, "Block-nerf: Scalable large scene neural view synthesis," in *Proceedings of the IEEE/CVF Conference on Computer Vision and Pattern Recognition*, 2022, pp. 8248–8258.
- [7] O. Özyeşil, V. Voroninski, R. Basri, and A. Singer, "A survey of structure from motion*," *Acta Numerica*, vol. 26, pp. 305–364, 2017.
- [8] R. Fan, X. Ai, and N. Dahnoun, "Road surface 3d reconstruction based on dense subpixel disparity map estimation," *IEEE Transactions on Image Processing*, vol. 27, no. 6, pp. 3025–3035, 2018.
- [9] S.-J. Yu, S. R. Sukumar, A. F. Koschan, D. L. Page, and M. A. Abidi, "3d reconstruction of road surfaces using an integrated multi-sensory approach," *Optics and lasers in engineering*, vol. 45, no. 7, pp. 808–818, 2007.
- [10] H. Brunken and C. Gühmann, "Road surface reconstruction by stereo vision," *PFG—Journal of Photogrammetry, Remote Sensing and Geoinformation Science*, vol. 88, no. 6, pp. 433–448, 2020.
- [11] S. Agarwal, Y. Furukawa, N. Snavely, I. Simon, B. Curless, S. M. Seitz, and R. Szeliski, "Building rome in a day," *Communications of the ACM*, vol. 54, no. 10, pp. 105–112, 2011.
- [12] T. Qin, Y. Zheng, T. Chen, Y. Chen, and Q. Su, "A light-weight semantic map for visual localization towards autonomous driving," in *2021 IEEE International Conference on Robotics and Automation (ICRA)*. IEEE, 2021, pp. 11 248–11 254.
- [13] M. Levoy and P. Hanrahan, "Light field rendering," in *Proceedings of the 23rd annual conference on Computer graphics and interactive techniques*, 1996, pp. 31–42.
- [14] M. Waechter, N. Moehrle, and M. Goesele, "Let there be color! large-scale texturing of 3d reconstructions," in *European conference on computer vision*. Springer, 2014, pp. 836–850.
- [15] H. Caesar, V. Bankiti, A. H. Lang, S. Vora, V. E. Liong, Q. Xu, A. Krishnan, Y. Pan, G. Baldan, and O. Beijbom, "nuscenes: A multimodal dataset for autonomous driving," in *Proceedings of the IEEE/CVF conference on computer vision and pattern recognition*, 2020, pp. 11 621–11 631.
- [16] A. Geiger, P. Lenz, C. Stiller, and R. Urtasun, "Vision meets robotics: The kitti dataset," *International Journal of Robotics Research (IJRR)*, 2013.
- [17] C. Campos, R. Elvira, J. J. G. Rodríguez, J. M. Montiel, and J. D. Tardós, "Orb-slam3: An accurate open-source library for visual, visual-inertial, and multimap slam," *IEEE Transactions on Robotics*, vol. 37, no. 6, pp. 1874–1890, 2021.
- [18] B. Cheng, I. Misra, A. G. Schwing, A. Kirillov, and R. Girdhar, "Masked-attention mask transformer for universal image segmentation," in *Proceedings of the IEEE/CVF Conference on Computer Vision and Pattern Recognition*, 2022, pp. 1290–1299.
- [19] N. Ravi, J. Reizenstein, D. Novotny, T. Gordon, W.-Y. Lo, J. Johnson, and G. Gkioxari, "Accelerating 3d deep learning with pytorch3d," *arXiv preprint arXiv:2007.08501*, 2020.
- [20] C. Quei-An, "Nerf-pl: a pytorch-lightning implementation of nerf," 2020. [Online]. Available: https://github.com/kweal23/nerf_pl/
- [21] Z. Liu, Y. Lin, Y. Cao, H. Hu, Y. Wei, Z. Zhang, S. Lin, and B. Guo, "Swin transformer: Hierarchical vision transformer using shifted windows," in *Proceedings of the IEEE/CVF International Conference on Computer Vision*, 2021, pp. 10 012–10 022.
- [22] G. Neuhold, T. Ollmann, S. Rota Bulò, and P. Kotschieder, "The mapillary vistas dataset for semantic understanding of street scenes," in *Proceedings of the IEEE international conference on computer vision*, 2017, pp. 4990–4999.
- [23] D. P. Kingma and J. Ba, "Adam: A method for stochastic optimization," in *International Conference on Learning Representations*, 2014.
- [24] Z. Wang, S. Wu, W. Xie, M. Chen, and V. A. Prisacariu, "Nerf-: Neural radiance fields without known camera parameters," *arXiv preprint arXiv:2102.07064*, 2021.